Cell Host & Microbe
Article

Coiled-Coil Domain-Dependent Homodimerization of Intracellular Barley Immune Receptors Defines a Minimal Functional Module for Triggering Cell Death

Takaki Maekawa,[1,8] Wei Cheng,[2,3,8] Laurentiu N. Spiridon,[4] Armin Töller,[1] Ewa Lukasik,[5] Yusuke Saijo,[1] Peiyuan Liu,[3] Qian-Hua Shen,[6] Marius A. Micluta,[4] Imre E. Somssich,[1] Frank L.W. Takken,[5] Andrei-Jose Petrescu,[4] Jijie Chai,[3,7,*] and Paul Schulze-Lefert[1,*]

[1]Department of Plant-Microbe Interactions, Max-Planck Institut für Pflanzenzüchtungsforschung, Carl-von-Linne Weg 10, 50829 Cologne, Germany
[2]Beijing Normal University, Haidian District, 19 Xinjiekouwai Street, 100875 Beijing, China
[3]National Institute of Biological Sciences, Number 7 Science Park Road, Zhongguancun Life Science Park, 102206 Beijing, China
[4]Department of Bioinformatics and Structural Biochemistry, Institute of Biochemistry of the Romanian Academy, Splaiul Independentei 296, 060036, Bucharest, Romania
[5]Department of Plant Pathology, Swammerdam Institute for Life Sciences, University of Amsterdam, Science Park 904, 1098 XH Amsterdam, The Netherlands
[6]State Key Laboratory of Plant Cell and Chromosome Engineering, Institute of Genetics and Developmental Biology, Chinese Academy of Sciences, Datun Road, Chaoyang District, 100101 Beijing, China
[7]College of Biological Sciences, Tsinghua University, Haidian District, 100084 Beijing, China
[8]These authors contributed equally to this work
*Correspondence: chaijijie@nibs.ac.cn (J.C.), schlef@mpipz.mpg.de (P.S.-L.)
DOI 10.1016/j.chom.2011.02.008

SUMMARY

Plants and animals have evolved structurally related innate immune sensors, designated NLRs, to detect intracellular nonself molecules. NLRs are modular, consisting of N-terminal coiled-coil (CC) or TOLL/interleukin-1 receptor (TIR) domains, a central nucleotide-binding (NB) domain, and C-terminal leucine-rich repeats (LRRs). The polymorphic barley mildew A (*MLA*) locus encodes CC-containing allelic immune receptors recognizing effectors of the pathogenic powdery mildew fungus. We report the crystal structure of an MLA receptor's invariant CC domain, which reveals a rod-shaped homodimer. MLA receptors also self-associate in vivo, but self-association appears to be independent of effector-triggered receptor activation. MLA CC mutants that fail to self-interact impair in planta cell death activity triggered by the CC domain alone and by an autoactive full-length MLA receptor that mimics its ATP-bound state. Thus, CC domain-dependent dimerization of the immune sensor defines a minimal functional unit and implies a role for the dimeric CC module in downstream immune signaling.

INTRODUCTION

Plants have evolved a multilayered innate immune system against microbial pathogens (Jones and Dangl, 2006). The first layer, termed microbe-associated molecular pattern (MAMP)-triggered immunity (MTI), limits the growth of potential microbial intruders upon MAMP perception by membrane-resident pattern recognition receptors. Successful pathogens, however, suppress MTI via the action of effectors delivered into host cells. Recognition of effectors by intracellular host resistance (R) proteins constitutes the second layer of the immune system, designated effector-triggered immunity (ETI), that typically leads to a localized host cell death response.

Most intracellular R proteins are modular consisting of N-terminal coiled-coil (CC) or TOLL/interleukin-1 receptor (TIR) domains, a central nucleotide-binding (NB) domain, and C-terminal leucine-rich repeats (LRRs). They are referred to as CNL or TNL, respectively, and belong to the NLR family of intracellular immune sensors in plants and animals. NLRs are a subfamily of signal transduction ATPases with numerous domains (STAND) NTPases found in archaea, bacteria, fungi, plants, and animals (Leipe et al., 2004). The NB domain is part of the central NB–ARC module shared between human apoptotic protease-activating factor 1 (APAF-1), R protein and *Caenorhabditis elegans* CED-4 (Lukasik and Takken, 2009). No TNL R proteins are found in monocotyledonous plants (Bai et al., 2002), suggesting that TNLs were lost in this lineage upon divergence from common angiosperm ancestors. By inference, the fundamental mechanism of CNL-mediated ETI should be conserved in angiosperms.

The polymorphic barley mildew A (*MLA*) *R* locus encodes functionally diversified CNL-type allelic immune receptors each recognizing a distinct isolate-specific effector of the pathogenic powdery mildew fungus, *Blumeria graminis* f. sp. *hordei* (*Bgh*, Seeholzer et al., 2010). MLA receptors share >90% sequence identity with most diversified selection sites residing in the C-terminal LRR domain, suggesting that the largely invariant CC and NB-ARC domains have invariant roles in MLA-triggered immunity (Seeholzer et al., 2010). Consistent with this, domain swap analyses between MLA1 and MLA6 revealed that the

C-terminal LRR domain, but not the CC or the NB parts, determines recognition specificity of *Bgh* effectors (Shen et al., 2003). Recognition of the *Bgh* effector AVR_{A10} by MLA10 induces nuclear associations between MLA and WRKY transcription factors likely through the MLA CC domain (Shen et al., 2007). Genetic evidence indicated that these WRKY factors negatively act in MTI against *Bgh*. Thus, the MLA-WRKY association appears to interfere with the WRKY repressor function, resulting in derepression of MTI (Shen et al., 2007). A subset of barley MLA resistance specificities genetically requires for their function the cochaperones RAR1 and SGT1 (Azevedo et al., 2002; Shirasu, 2009; Shirasu et al., 1999). SGT1 and cytosolic HSP90, but not RAR1, interact specifically with the MLA LRR domain. Together these proteins positively regulate MLA receptor maturation (Bieri et al., 2004; Shirasu, 2009).

Similar to APAF-1, CED-4, and human NODs, some plant R proteins form homomeric assemblies prior to or post effector recognition (Ade et al., 2007; Danot et al., 2009; Gutierrez et al., 2010; Mestre and Baulcombe, 2006). The studies of N (TNL), RPS5 (CNL), and Prf (novel N-terminal domain) immune sensors provided evidence for homo-oligomerization through their N-terminal domains, although neither the structural basis for this nor its significance in ETI are known. Furthermore, no crystal structure of an R protein is available to date, although recently the structure of a TIR domain from an *Arabidopsis* non-R protein has been resolved and found to be a monomer (Chan et al., 2010). Here we report the crystal structure of the invariant CC domain of MLA and address the significance of its homo-oligomerization. Our data provide mechanistic clues to how CNL proteins contribute to ETI.

RESULTS

Recombinant MLA10 CC Domain Forms a Homodimer

The CC domain of $MLA10_{5–120}$ was expressed in *Escherichia coli* and purified to homogeneity for crystallization. The crystal structure of the CC domain was determined at 2.0 Å resolution by single-wavelength anomalous diffraction (SAD) (see Table S1 available online). The final atomic model contains residues 6–120. No electron density was observed corresponding to the five residues 91–95, likely due to their residual local flexibility in the crystal (Figures 1A and 1B).

As predicted from the primary sequence, the monomeric structure of the CC domain is mainly α helical and contains two long antiparallel α helices linked by a short loop (Figure 1C), thereby forming a helix-loop-helix structure. Although the hydrophobic residues predominantly line their interior sides, the two α helices pack loosely against each other. Therefore most of the two α helices are located apart, and only marginal contacts are made between the N-terminal portion of α1a and the N-terminal portion of α2b. Such interactions, however, appear insufficient to stabilize the two seemingly independent α helices, suggesting that other protein-protein interactions may be involved to this end. Our analysis identified a strong candidate dimer interface. In the crystals, two protomers of the CC domain pack symmetrically mainly through the interior-lined residues in the CC monomer (Figure 1A). Assembly of the CC domain dimer resembles two springs slammed together, and such an intertwined packing arrangement gives rise to an extensive dimer interface, generating the burial of 7950 $Å^2$ surface area (Figure 1A). This large buried surface area suggests that the CC domain dimer would be highly stable and likely intrinsically inseparable. Dimerization of the CC domain creates a rod-shaped molecule, with one helical bundle at each end (Figure 1A). Strikingly different electrostatic properties exist for the two opposite sides of the dimer (Figure S1). The overall dimensions of the dimer are approximate length 90 Å, height 20 Å, and width 20 Å, as measured by the corresponding backbone carbon atoms.

A large portion of the two α helices is involved in homodimerization of the CC domain. The helix α1 (residues 12–44) forms a parallel two-stranded CC fold in the dimer structure (Figure 2A). In strong support of the structural observation, a prediction made by the program COILS gave a score of ~0.95 for residues 26–56 to fold into a CC structure. CC formation in the CC domain is primarily dependent on Ile12, Leu15, Leu19, Glu22, His26, Val29, Ile33, Leu36, Leu40, and Met43 from the heptad repeat sequences (Figure 2A). These residues are located either at a or d (Figure 1C) positions that make hydrophobic contacts with those from the other helix, which are characteristic of the interactions observed in other CC structures (Kohn et al., 1997). Failure to detect residues 12–22 for CC formation by the program may have arisen from the nonhydrophobic residue Glu22. However, Glu at position d (Figure 1C) has been observed in other CC structures. The ends of the CC splay apart slightly and, together with the N-terminal half of helix α2b and the C-terminal third of helix α2a, form short antiparallel four-helix bundles (Figure 2B). In total, 20 residues from both CC protomers form a network of van der Waals interactions within one helical bundle. Leu11, Leu15, Leu18, Phe99, Met103, and Ser106 from one monomer and Leu36, Glu39, Met43, Ser73, Ile76, and Val80 from the other one, that reside at the center of one helical bundle, constitute the core of hydrophobic interactions within one helix bundle (Figure 2B). To further strengthen dimerization of the CC domain, the proximal C-terminal end of α2b makes tight hydrophobic contacts with the C-terminal end of α1a and the N-terminal end of α2a from the other CC monomer (Figure 2C). In addition, the electrostatic interaction between Lys116 and His117 from the loop C-terminal to the helix α2a in one monomer and Asp59 and Asp62 in the other monomer contribute to CC domain dimerization, respectively (Figure 2C).

MLA Self-Association In Planta

To study potential MLA self-association in planta by coimmunoprecipitation (coIP) experiments, we generated stable transgenic barley plants coexpressing *MLA1-HA* and *MLA1-Myc*. For this purpose, we crossed single-copy transgenic lines each expressing a functional *MLA1-HA* or *MLA1-Myc* under 5′ native regulatory sequences (Bieri et al., 2004). The *MLA1-HA* and *MLA1-Myc* coexpressing plants showed race-specific resistance against *Blumeria graminis* isolates K1, but not A6, (containing or lacking Avr_{A1}, respectively; data not shown). IP of MLA1-Myc from soluble total leaf extracts of these lines using anti-Myc antibodies also recovered MLA1-HA, demonstrating coIP of MLA1-HA and MLA1-Myc (Figure 3A, right). By contrast, IP using control IgG from extracts of the coexpressing plants failed to detect MLA1-HA (Figure 3A, right), verifying the specificity of the above coIP. Thus, our results indicate MLA1 self-association in planta.

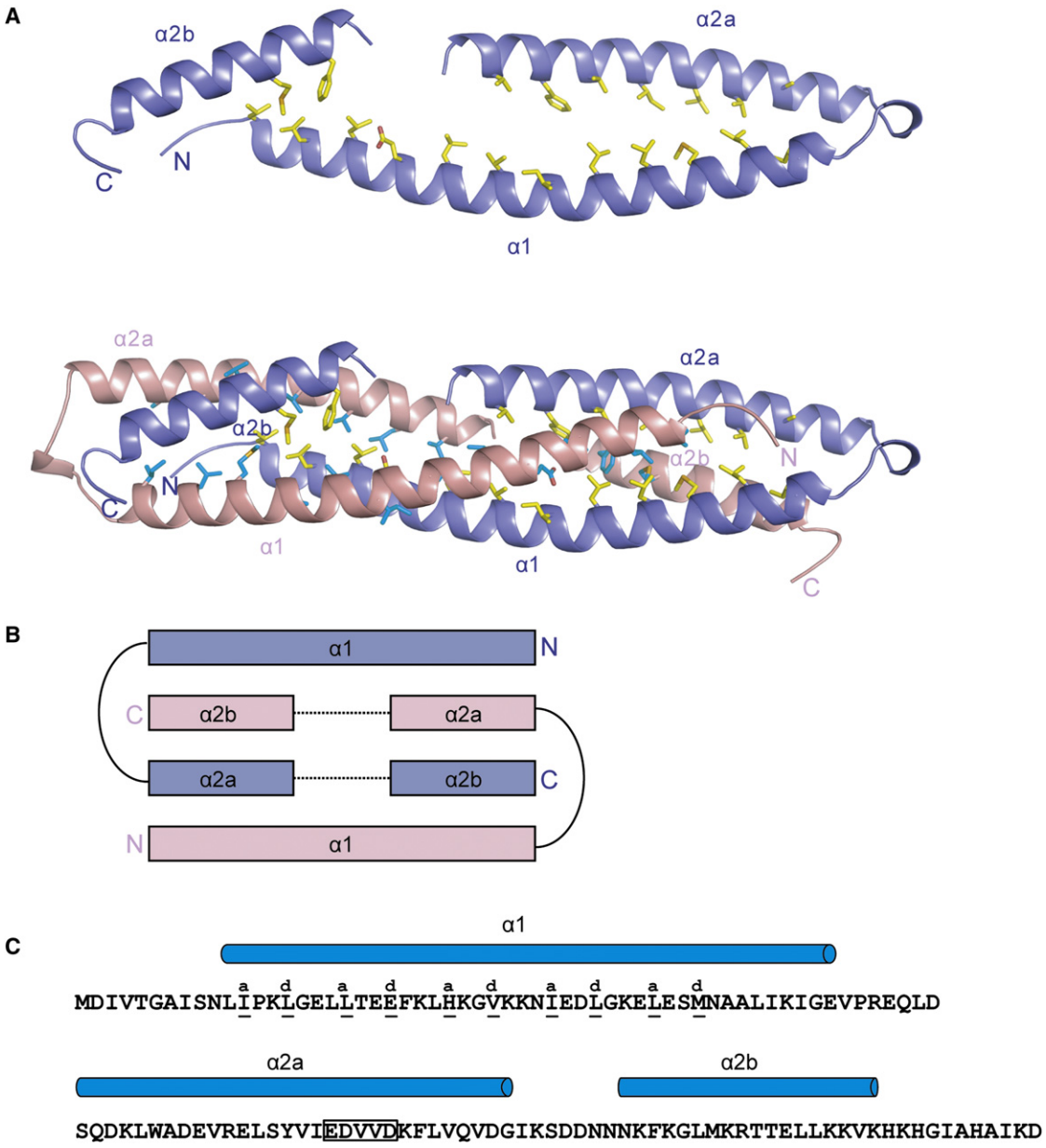

Figure 1. The Coiled-Coil Domain of MLA10 Forms a Homodimer in the Crystal Structure

(A) Cartoon representation of the monomer structure of the CC domain from MLA10. A monomer contains three helices, labeled with α1, α2a, and α2b (top panel). The three helices dimerize through an extensive interface (bottom panel). The residues involved in homodimerization are shown by yellow and cyan sticks. The two monomers are colored in slate and pink.

(B) A diagram for the topology of the dimer showing pairwise interactions of the helices.

(C) Sequence of the CC domain, with the helices shown in cylinders on top. Residues that follow the pattern of heptad repeat are underlined. The letters "a" and "d" represent their positions in the heptad repeat. The conserved "EDVID" motif is indicated by the black box.

Next we examined whether MLA1 self-association is dependent on MLA1-induced immune responses. Total leaf protein extracts of the coexpressing plants were prepared at several time points after inoculation with the *Bgh* isolates K1 or A6 (incompatible or compatible interactions, respectively; Figure 3B). The amount of coimmunoprecipitated MLA1-HA gradually increased after challenge with both isolates (Figure 3B). This corresponded with a similar elevated IP of MLA1-Myc and was correlated with the pathogen-inducible increase of total MLA1-HA and MLA1-Myc (Figure 3B). These results indicate that MLA1 self-association is not the consequence of AVR_{A1}-dependent receptor activation, but occurs in naive and infected plants. Furthermore, this suggests that MLA1 self-association is not disrupted upon perception of the cognate fungal effector.

We performed gel filtration analyses of leaf cell extracts derived from the transgenic line expressing *MLA1-HA* by applying

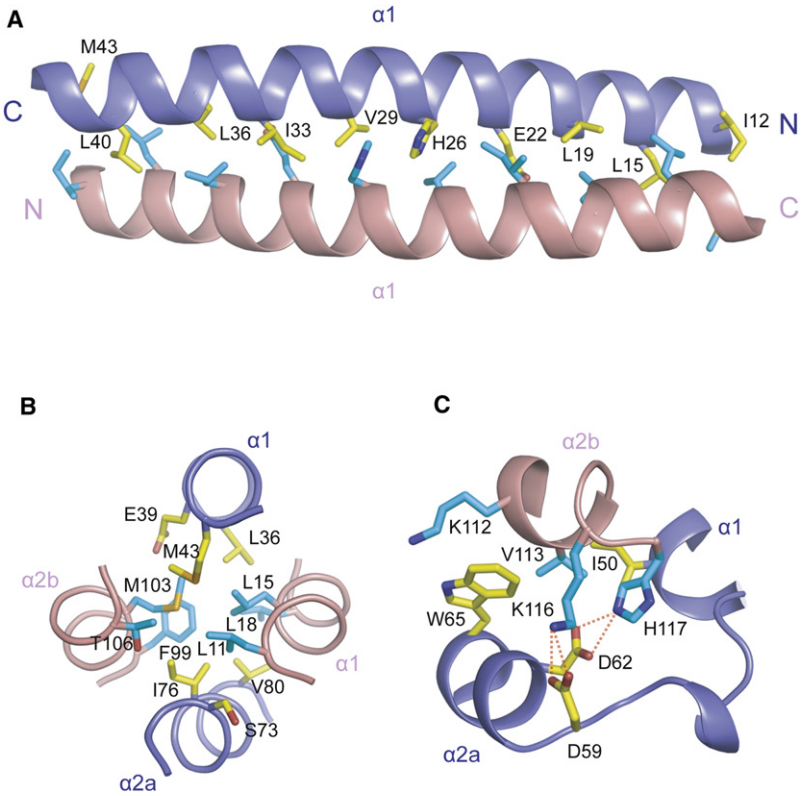

Figure 2. Detailed Interactions Involved in Homodimerization of MLA10 CC Domain

(A) The CC interactions between the two α1 helices. The side chains from the tow monomers are shown in stick and colored in yellow and cyan, respectively. The color codes are the same for (B) and (C).

(B) Detailed interactions involved in the four-helix bundle formed by the α2a, α2b, and two α1 helices.

(C) Detailed interactions around one end of the homodimer involving the helix-turn-helix (α1, α2a) and α2b.

almost identical protein extraction conditions used in the aforementioned coIP experiments. No significant changes in the apparent size of a 300–400 kDa complex were observed upon *Bgh* inoculation during compatible or AVR_{A1}-dependent incompatible interactions. Under the experimental conditions tested, MLA1-HA was barely detectable in fractions corresponding to its monomeric size (105 kDa). However, the peak size of the MLA complex was reduced to an apparent size of ~200 kDa in a buffer containing high NaCl concentrations (Figure 3C, lower panel). The reduced peak size was still larger than monomeric MLA (Figure 3C, lower panel), indicating incomplete complex dissociation. Of note, essentially the same MLA1-HA profiles were obtained with total extracts derived from leaf epidermal peels, indicating the presence of the MLA1 complex(es) in cells that are in direct physical contact with the fungus (Figure S2). Thus, the vast majority of MLA1 forms (a) 300–400 kDa complex(es) in planta that are not disrupted by the fungal trigger. It is possible that these include MLA self-association seen by coIP, since both methods detect complexes independent of AVR_{A1}-dependent receptor activation.

Structure-Guided Mutagenesis of the MLA10 CC Domain

To further investigate the role of the CC domain in MLA self-association, we first employed the yeast two-hybrid assay. Coexpression of identical truncated MLA10 variants fused to prey or bait constructs revealed self-interactions of $MLA10_{1\text{-}225}$. We failed to detect self-interactions of MLA10 full-length, $MLA10_{1\text{-}523}$, and $MLA10_{1\text{-}46}$ (Figure 4A). Lack of interaction with the former two truncated MLA10 proteins likely reflects their instability following expression in yeast (Figure S3). Therefore we used $MLA10_{1\text{-}225}$ for subsequent detailed analyses.

To define the functional significance of the dimeric interface found in the CC structure (Figures 1 and 2), individual residues lining the interior between the protomers of the CC dimer were substituted to glutamic acid (Figure 4B). Substitution of these residues is predicted to be thermodynamically unfavorable, possibly destabilizing the dimeric structure. Of 17 targeted single substitutions, three located in helix α1 (I33E, L36E, and M43E) resulted in loss of $MLA10_{1\text{-}225}$ self-interaction, whereas interactions were still detectable to varying degrees upon coexpression of eight other variants (L11E, L15E, L18E, L25E, V29E, V69E, L72E, and I76E; Figure 4C). Due to autoactivity of the bait (yeast cells grew in the absence of prey on selection medium; data not shown), the colony growth phenotype of five substitutions (L19E, F23E, F99E, M103E, and L110E) could not be examined. We confirmed that all tested substitution derivatives accumulated in yeast (Figure S3). Collectively, these data imply that CC substitutions in helix α1 disrupt MLA10 self-interaction while most substitutions in helix α2a and α2b weaken this interaction.

We tested CC dimer formation in solution by gel filtration chromatography. The recombinant ~13 kDa wild-type CC domain ($MLA10_{5\text{-}120}$) coeluted with a 25.6 kDa size marker, indicating that the MLA CC domain exists exclusively as dimer in solution (Figure 4D). Dimer formation of the recombinant wild-type CC domain in solution was confirmed using chemical cross-linkers, bis [Sulfosuccinimidyl] suberate (BS3) and ethylene glycolbis (sulfosuccinimidyl-succinate) (Sulfo-EGS), followed by separation on SDS-PAGE (Figure 4E). Notably mutations of residues at the dimer interface (L11E, I33E, L36E, M43E, V69E, L72E, I76E, and L110E) resulted in insoluble or highly unstable CC variants (data not shown), which is consistent with their presumed role in CC dimer formation/stability.

To examine the significance of the single amino acid substitutions in MLA10-triggered immunity, we expressed full-length MLA10 in a transient single-cell expression system in barley leaf epidermal cells (Shen et al., 2007). We scored MLA10-specified disease resistance upon inoculation with the *Bgh* A6 isolate expressing cognate Avr_{A10} by determining the frequency of fungal haustorium formation inside single host cells (haustorium index; Shen et al., 2007). Constructs of wild-type MLA10 or the

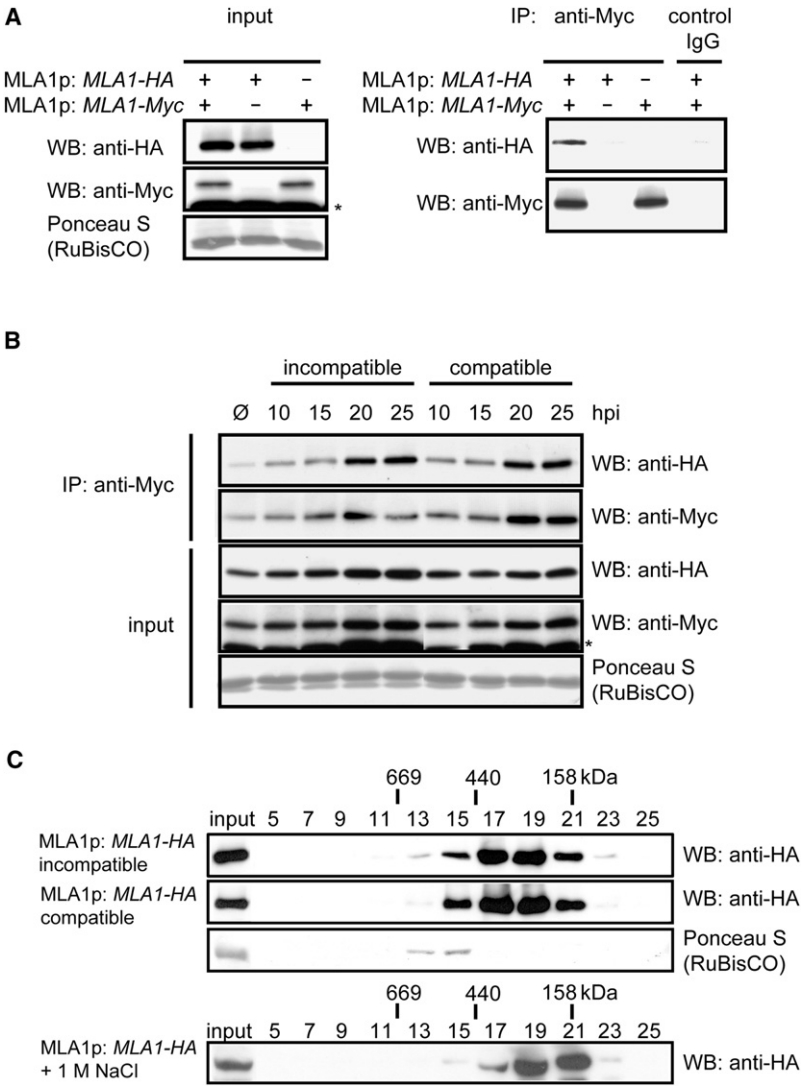

Figure 3. MLA Self-Associates In Planta

(A) CoIP of total leaf protein extracts of transgenic barley plants expressing MLA1-HA and/or MLA1-Myc under their native 5′ regulatory sequences. The samples were prepared at 17 hr postinoculation (hpi) with *B. graminis* conidiospores of the avirulent isolate K1 expressing AVR_{A1}. Asterisk indicates nonspecific signals.

(B) Activation-independent in planta self-association. Total leaf protein extracts were prepared at the indicated time points (hpi) after inoculation with the *B. graminis* avirulent isolate K1 expressing AVR_{A1} or the virulent isolate A6 lacking AVR_{A1} (incompatible or compatible, respectively). Ø, noninoculated controls. Asterisk indicates nonspecific signals.

(C) MLA exists in high molecular weight complex(es) in planta. Gel filtration analyses of soluble cell extracts of leaf material derived from transgenic barley lines containing a functional single-copy HA epitope-tagged *MLA1* under the control of native 5′ regulatory sequences. Seven-day-old detached leaves were noninoculated or inoculated with the avirulent or virulent *B. graminis* isolates (see B) for 24 hr before soluble cell extracts were prepared. Molecular sizes (in kDa) of the indicated fractions are shown uppermost. Fraction numbers are shown directly below. Gel filtration fractions derived from leaf material was subjected to immunoblot analyses with HA-specific antiserum (top two panels) or Ponceau S staining to visualize RuBisCO complexes (third panel). Gel filtration fractions of noninoculated leaf material prepared in a buffer containing 1 M NaCl were subjected to immunoblot analyses with HA-specific antiserum (lowermost panel). Note that the peak size of the MLA complex was reduced to an apparent size of ~200 kDa in the high salt buffer.

MLA10 CC substitution variants described above, each fused at the C terminus to yellow fluorescence protein (YFP), were biolistically codelivered with a GUS reporter construct (Figure 4F). We also tested a MLA10 CC variant, G37R, which represents a naturally occurring G to R polymorphism in α1 of the CC of the MLA34 resistance specificity (Seeholzer et al., 2010). MLA10-YFP and all tested mutant derivatives showed YFP fluorescence signals inside leaf epidermal cells 24 hr after biolistic delivery, indicating expression and accumulation of the fusion proteins (data not shown). Nearly all tested MLA10 variants lost disease resistance activity, except L18E and G37R derivatives that retain wild-type-like MLA10 immunity (Figure 4F). Upon codelivery of GUS and F99E, reporter gene expression was barely observable, suggesting that this variant may trigger a host cell death response that prevents sufficient GUS accumulation (Figure 4F). The loss of MLA10 immunity seen upon expression of most of the tested MLA10 CC variants indicates functional importance and vulnerability of the MLA10 CC domain to such single substitutions. Together with the exceptional CC sequence conservation among functionally diversified MLA resistance specificities (Seeholzer et al., 2010), this suggests the existence of invariant functional constraints acting on this domain.

Interestingly, most of the $MLA10_{1-225}$ prey variants, including those with disrupted CC self-association, showed impaired interactions with the truncated *Hv*$WRKY1_{260-353}$ bait, except for L18E (Figure 4C). However, the $MLA10_{1-46}$ fragment, containing most residues of helix α1 of the CC domain, was previously shown to be necessary and sufficient for the MLA-*Hv*WRKY1 interaction (Shen et al., 2007). Since helix α1 of the CC domain alone is unlikely to form a stable dimer and $MLA10_{1-46}$ does not self interact (Figures 1A and 4A), CC dimerization per se cannot be essential for the heteromeric association but might regulate the accessibility of the $MLA10_{1-46}$ region for the interaction with the transcription factor. Notably, the MLA CC L18E variant is the only targeted substitution that retains both disease resistance and interaction with *Hv*WRKY1 (Figures 4C and 4F). Together this corroborates a link between disease resistance activity, CC dimerization, and interaction with the transcription factor and implies that the MLA CC dimer acts as functional unit in the immune response.

Monomeric Full-Length MLA27 Binds ADP

To characterize nucleotide binding of MLA in the context of the full-length protein, we expressed 20 cDNAs, each encoding

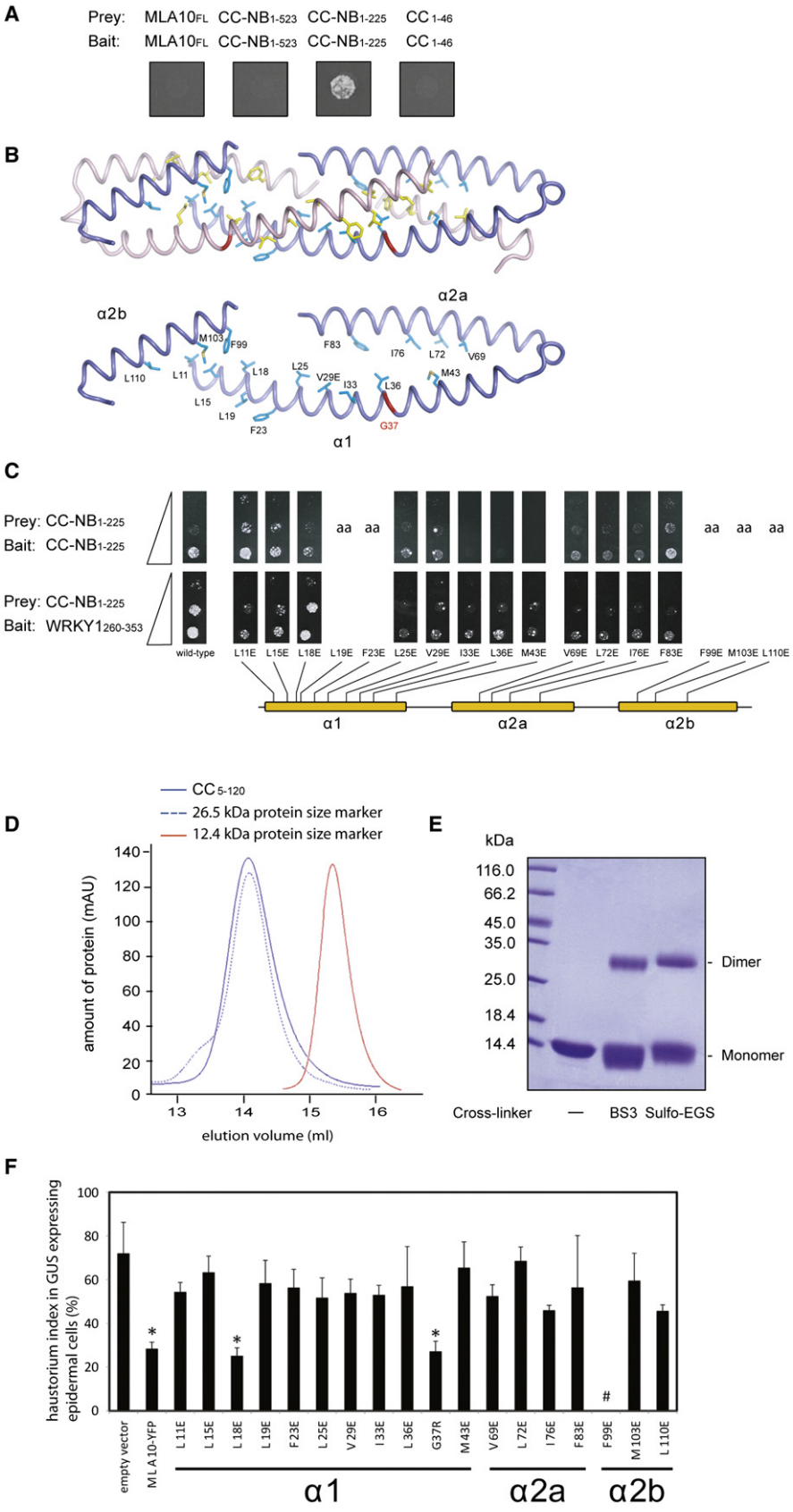
A
Prey: MLA10FL CC-NB1-523 CC-NB1-225 CC 1-46
Bait: MLA10FL CC-NB1-523 CC-NB1-225 CC 1-46
B
α2b
α2a
α1
C
Prey: CC-NB1-225
Bait: CC-NB1-225
Prey: CC-NB1-225
Bait: WRKY1260-353
wild-type
L11E L15E L18E L19E F23E L25E V29E I33E L36E M43E V69E L72E I76E F83E F99E M103E L110E
aa aa
aa aa aa
α1
α2a
α2b
D
CC 5-120
26.5 kDa protein size marker
12.4 kDa protein size marker
amount of protein (mAU)
elution volume (ml)
E
kDa
116.0
66.2
45.0
35.0
25.0
18.4
14.4
Dimer
Monomer
Cross-linker — BS3 Sulfo-EGS
F
haustorium index in GUS expressing epidermal cells (%)
empty vector
MLA10-YFP
L11E L15E L18E L19E F23E L25E V29E I33E L36E G37R M43E V69E L72E I76E F83E F99E M103E L110E
α1
α2a
α2b

a naturally occurring MLA receptor variant in heterologous prokaryotic and eukaryotic expression systems. Only one resistance specificity, MLA27, was successfully purified to homogeneity following expression in insect cells. Purified MLA27 was subsequently subjected to gel filtration chromatography. Interestingly, the filtration profile showed a single peak between 66 and 200 kDa size marker proteins, indicating that MLA27 elutes exclusively as an ~105 kDa monomer (Figure 5A).

To assess proper folding of full-length MLA27, its ability to bind nucleotides was examined (Figure 5B). A luciferase-based ATP/ADP identification and quantification method was employed. A boiling method was used to release any bound nucleotides from the protein. Despite the high sensitivity of the assay (detection level <<1 pmol of ATP), no ATP was detected in the extract of 70 pmol MLA27. For ADP detection, the assay was extended by adding phosphoenol pyruvate and pyruvate kinase, which converts ADP back to ATP. Since MLA27 was purified in a buffer containing 5 μM ADP, direct assaying for the presence of protein-bound ADP was not possible. To remove unbound nucleotides, MLA27 was subjected to gel filtration chromatography and the resulting fractions were analyzed for the presence of ADP and protein. Bovine serum albumin (BSA) dissolved in the same ADP-containing buffer served as a reference. Both BSA and MLA27 eluted between 200 and 600 μl and peak at approximately 400 μl. No ADP was detected in the fractions eluting from the BSA-loaded column, but in the MLA-containing fractions ADP was present and its elution profile corresponded to that of the protein (Figure 5B). We calculated the total amount of coeluting ADP (202 ± 26 pmol) to be ~43% of that of MLA27 (471 ± 42 pmol). Assuming that NB-ARC proteins such as MLA27 have one NB site, this indicates an occupancy of the protein with ADP of around 43%.

Notably, the ADP concentration remained elevated in the late fractions after the MLA27-containing peak. We assumed that this ADP has dissociated from the protein while migrating through the column. Free ADP migrates more slowly and therefore elutes in later fractions. This hypothesis is consistent with the observation that ADP was not detected in the corresponding BSA reference fractions until elution of the column void volume (±1 ml). ADP concentration measurements in the fractions eluting between 200 and 900 μl subtracted with the BSA control values revealed a total amount of 289 ± 42 pmol ADP in the eluate. This amount corresponds to 61% of the amount of MLA eluting and implies that a third of the nucleotide has dissociated while migrating through the column. As the protein first elutes around 5 min, this would be consistent with a relatively stable MLA27-ADP complex with a half-life exceeding 5 min. Taken together, we conclude that at least 61% of the purified MLA27 protein is ADP bound, indicating that the NB domain of the bulk of the purified full-length immune receptor is properly folded.

CC-Dependent MLA10 Self-Association Is Required for Full Activation of Cell Death in *N. benthamiana*

The perception of cognate effectors followed by replacement of ADP by ATP at the NB domain of R proteins is proposed as a general receptor activation mechanism to initiate an immune response (Takken et al., 2006). Autoactivating mutations, i.e., independent of ligand, are frequently found at the conserved MHD motif in the NB domain (van Ooijen et al., 2007), leading in plants to a cell death response conventionally used as an immune response proxy. Since P loop mutations in MLA10 result in loss-of-disease resistance activity (data not shown) and full-length MLA27 monomer was shown to bind ADP (Figure 5B), we suspected on the basis of a structural MLA NB model (Figure S4) that substitutions at the conserved MHD motif would render the receptor autoactive. Transient gene expression of the MHD motif variant MLA10 D502V in barley leaf epidermal cells resulted in a reduction of reporter expression (red fluorescence protein [RFP]-mediated fluorescence) compared to wild-type, possibly reflecting autoactivation-triggered cell death (Figure 6A).

To test the potential cell death activity of MLA10 D502V quantitatively, we expressed the receptor in *Nicotiana benthamiana* by *Agrobacterium*-mediated delivery of the expression vector and measured electrolyte leakage of the plant cells at 24 and 48 hr post *Agrobacterium* infiltration (hpi) in leaf disks (Figure 6B). In comparison to wild-type MLA10, the D502V variant induced a marked conductivity increase at 48 hpi (Figure 6B), suggesting cell death activity due to receptor autoactivation in this heterologous expression system. To assess the role of single MLA10 CC substitutions that were shown to abolish both CC homomeric interactions in the yeast two-hybrid experiments and loss of disease resistance activity

Figure 4. Structure-Guided Mutagenesis of the MLA10 CC Domain

(A) MLA10 CC self-interactions in yeast. Representative results of yeast two-hybrid assays between bait fusions of the LexA DNA-binding domain and prey fusions of the B42 activation domain containing identical truncated MLA10.

(B) Structure of MLA10 CC homodimer (top) and a monomer (bottom). Hydrophobic amino acids at the dimer interface are indicated. The naturally occurring G to R polymorphism at amino acid position 37 in MLA34 (Seeholzer et al., 2010) is shown in red.

(C) Single amino acid substitutions in the CC domain disrupt MLA10 CC self-interactions in yeast. Hydrophobic amino acids indicated in (B) were substituted to glutamate. aa, autoactivity of the bait construct alone (yeast cells grew in the absence of prey on selection medium; data not shown), the colony growth phenotype could not be examined.

(D) The recombinant wild-type CC domain of $MLA10_{5-120}$ exists exclusively as a dimer. The CC domain was expressed in *E. coli* and the purified protein was subsequently separated on a Superdex 75 gel filtration column in a buffer containing 100 mM NaCl. The wild-type CC domain (predicted molecular size, ~13 kDa) coeluted with a 25.6 kDa protein size marker.

(E) Chemical crosslinking confirmed a dimer formation of the recombinant wild-type CC domain in solution. The recombinant protein was incubated with either crosslinker BS3 or Sulfo-EGS in a buffer containing 100 mM NaCl. The protein samples were subjected to SDS-PAGE.

(F) Disease resistance activity of wild-type MLA10 and MLA10 CC substitution variants. Disease resistance activity was scored directly by determining the haustorium index in barley leaf epidermal cells upon biolistic codelivery of the indicated plasmid vectors and GUS reporter. Bombarded leaves were inoculated with *B. graminis* expressing AVR_{A10}. Fungal haustoria were microscopically scored 36 hr after spore inoculation. Data show average and SD from three independent experiments. Asterisk indicates significant differences from empty vector ($p < 0.01$). #, upon codelivery of GUS and F99E, the reporter gene expression was barely observable.

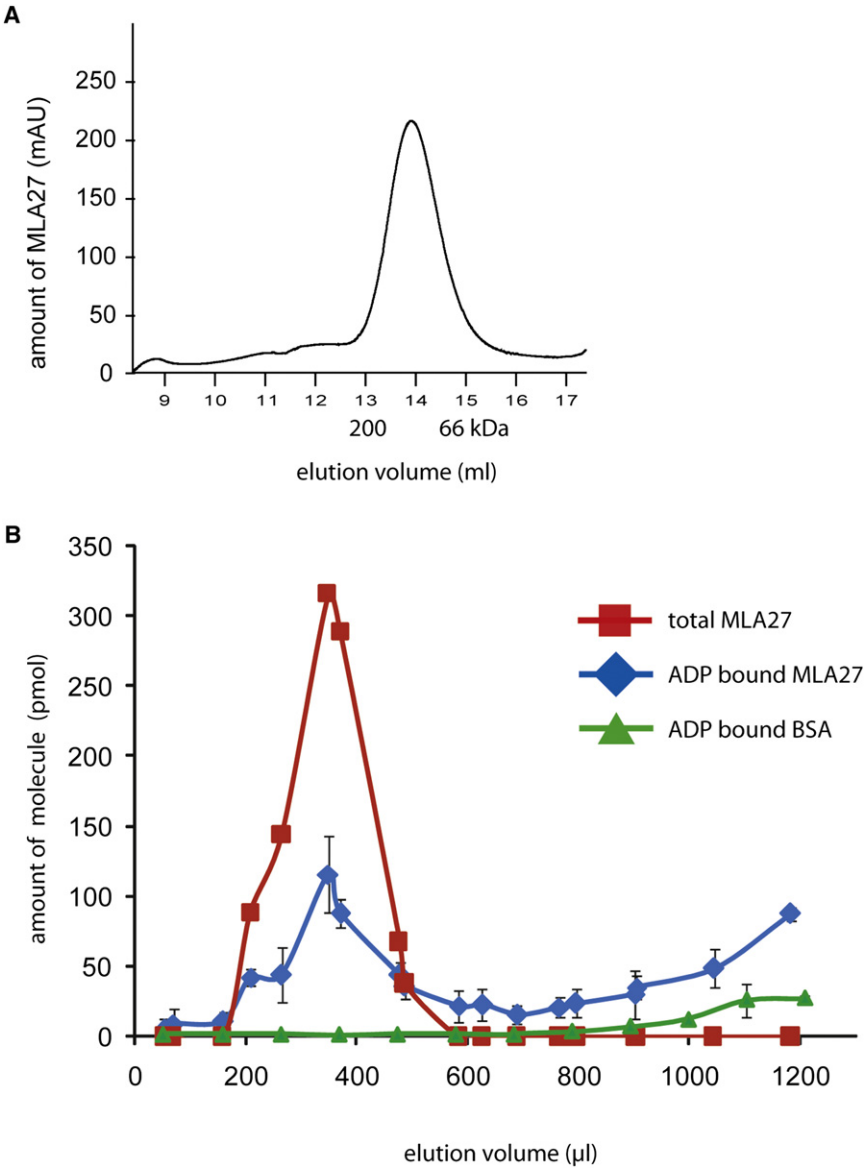

Figure 5. Monomeric Full-Length MLA27 Binds ADP

(A) MLA27 exists as a monomer following purification from insect cells. MLA27 was expressed in insects cells (SF21) and purified. The purified MLA27 protein was subsequently separated on a Superdex 200 gel filtration column. The position of calibration proteins are indicated in kDa.

(B) MLA27 binds ADP in vitro. Purified MLA27 was separated on a NAP5 size-exclusion column, and the amount of protein and ADP in each fraction was determined. MLA27 and BSA eluted in the same fractions. ADP exclusively coeluted with MLA27. Data show average and SD of two replicates from two independent experiments.

(I33E, L36E, and M43E; Figures 4C and 4F), we introduced the autoactivating substitution D502V in the context of these CC substitutions (D502V+I33E, D502V+L36E, and D502V+M43E, respectively; Figure 6B). Strikingly, each of the three double substitution variants suppressed the MLA10 D502V-mediated cell death activity (Figure 6B). This suppression was not the result of altered receptor abundance (Figure 6B, insert). Together with the activation-independent MLA self-association in vivo (Figure 3), this finding suggests that CC domain-dependent dimerization (Figure 1) is necessary for immune receptor activity leading to host cell death.

To further assess the significance of CC domain-dependent MLA dimerization in the cell death response, we tested cell death activity of the CC domain alone ($MLA10_{1-160}$) including the linker region between the CC and the NB-ARC domains (Figure S4). Surprisingly, the wild-type CC-domain was sufficient to induce a marked conductivity increase, whereas the CC substitutions (I33E, L36E, and M43E) failed to trigger the cell death response (Figure 6C). A truncated CC variant ($MLA10_{1-46}$) that does not self-interact in yeast (Figure 4A) also failed to trigger cell death (Figure 6C), although this fragment was previously shown to be necessary and sufficient for the MLA-*Hv*WRKY1 interaction (Shen et al., 2007). Collectively, these data suggest that the MLA CC dimer serves as minimal functional receptor unit for initiation of the cell death response.

DISCUSSION

Several NB-ARC proteins in vertebrates including APAF-1, CED-4, and human NODs are known to self-associate through their N-terminal and/or central NB-ARC domains (Danot et al., 2009; Qi et al., 2010). Previous studies in plants on N, RPS5, and Prf immune receptors indicate that their N-terminal domains provide a self-association platform for homo-oligomerization (Ade et al., 2007; Gutierrez et al., 2010; Mestre and Baulcombe, 2006). Our study identified the MLA CC domain as a homodimerization module with an autonomous folding capacity in solution (Figures 1, 2, and 4). Unlike in vertebrates, self-association of the NB-ARC domain has been rarely observed in plant NB-ARC proteins (Ade et al., 2007). This indicates a unique self-association property of the plant NLRs, which in turn might reflect distinct evolutionary fusions of N-terminal domains (CC/TIR versus CARD/PYD/BIR domains) to the shared NB-ARC domain in both phyla (Shen et al., 2007; Shen and Schulze-Lefert, 2007). APAF-1, CED-4, and plant N are known to form higher-order assemblies upon receptor activation (Mestre and Baulcombe, 2006; Qi et al., 2010; Yu et al., 2005). In contrast, we detected no higher-order MLA assemblies in gel filtration chromatography upon effector-dependent receptor activation (Figure 3C; Figure S2). Thus, if such MLA complexes exist, these must be unstable and/or transient in nature.

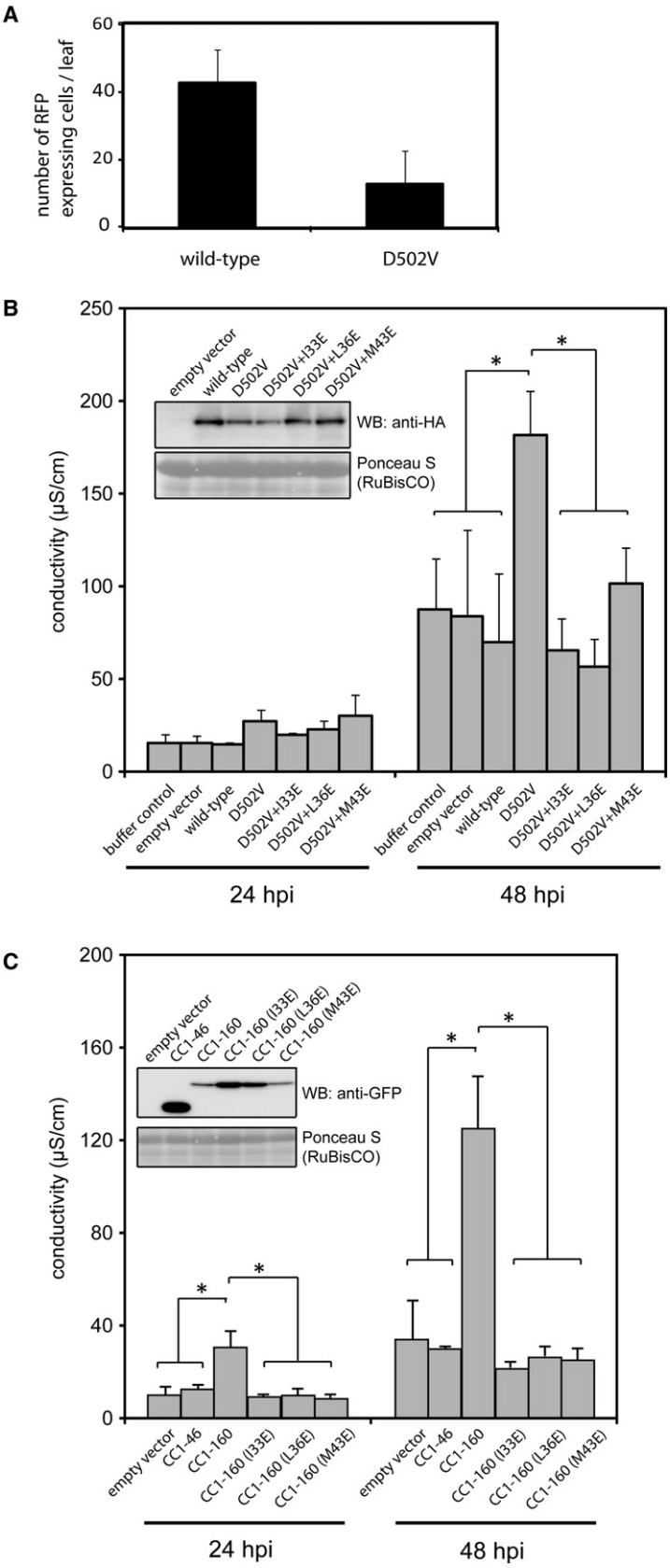

Figure 6. MLA10 Self-Association at the CC Domain Is Required for Cell Death Activation

(A) Reporter gene expression upon biolistic codelivery of plasmids containing wild-type MLA10-YFP or the MHD motif variant MLA10 (D502V)-YFP and RFP reporter in barley leaf epidermal cells. RFP-expressing cells were microscopically scored 48 hr after biolistic delivery. Data show average and SD of nine detached leaves from two independent experiments. These are significantly different (t test, $p < 0.01$).

(B) Quantification of cell death activity of MLA10 variants in *Nicotiana benthamiana*. Leaf disks from *N. benthamiana* were obtained at 22 hr after infiltration of *Agrobacterium tumefaciens* GV3101 ($OD_{600} = 0.1$) harboring the MLA10 autoactivating mutation (D502V) and/or self-association impaired mutations (shown in Figure 4) as indicated. Electrolyte leakage was measured at 24 and 48 hpi. Data show average and SD of more than four replicates from two independent experiments. The insert in the graph shows protein accumulation of the individual HA epitope-tagged MLA10 variants determined by western blot analyses. Total leaf protein extracts were prepared at 22 hr after *Agrobacterium* infiltration. Asterisk indicates significant difference ($p < 0.01$).

(C) Quantification of cell death activity of the indicated wild-type and mutant MLA10 CC domains in *N. benthamiana*. Electrolyte leakage was measured as described in Figure 6B. Data show average and SD of more than four replicates from two independent experiments. The insert in the graph shows protein accumulation of the indicated MLA10 CC variants fused to YFP determined by western blot analyses. Asterisk indicates significant difference ($p < 0.01$).

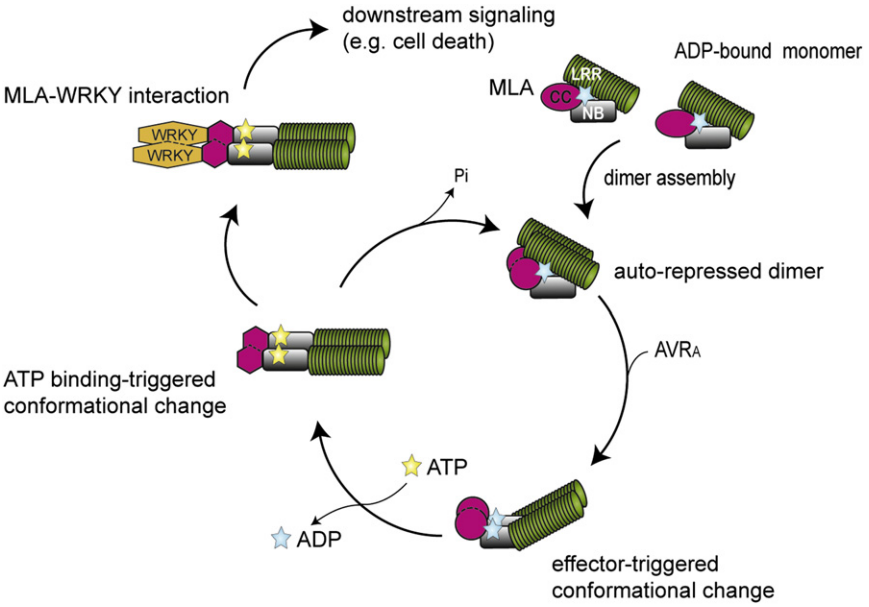

Figure 7. Schematic Representation of the MLA CC Dimer Initiating Downstream Signaling

ADP-bound MLA monomers are assembled into a homodimer by the large buried surface area generated at the CC protomer-protomer interface in combination with a plant-encoded folding machinery. Perception of cognate effector (AVR_A) at the LRR domain induces an initial conformational change in the NB-ARC (NB) domain, allowing replacement of ADP by ATP. Subsequently, a second conformational change in the self-interacting CC domains of the receptor dimer is thought to enable downstream signaling. It is possible that effector-triggered conformational changes of MLA CC dimers induce proximity of particular WRKY oligomers for downstream signaling (e.g., cell death).

We found a tight link between CC domain-dependent MLA self-association in the context of the full-length receptor and cell death activity (Figure 6). Combined with the crystal structure information of the MLA CC domain, we propose that the MLA homodimer defines a minimal functional receptor unit for triggering cell death. However, full-length MLA27 from insect cells was purified as a monomer (Figure 5A). It is possible that MLA dimerization/complex formation in planta is partly driven by the large buried surface area (7950 $Å^2$) generated at the CC protomer-protomer interface (Figure 1) in combination with a plant-encoded folding machinery including HSP90-RAR1-SGT1 (Bieri et al., 2004; Shirasu, 2009). Very few studies have directly examined nucleotide binding to plant NLRs. Biochemical analysis of autoactivating mutations of the tomato I-2 CNL-type R protein showed in vitro markedly reduced ATP hydrolysis but did not affect nucleotide binding (Tameling et al., 2006), suggesting that the ATP bound form is the "on state" while ATP hydrolysis switches the protein back to the "off state." However, these data were generated with truncated I-2 lacking the C-terminal LRR domain. We detected exclusively ADP bound to in vitro purified full-length MLA27 from insect cells (Figure 5), indicative of a stable inactive receptor monomer. Since wild-type I-2 lacking the LRR domain can bind ATP and ADP (Tameling et al., 2002, 2006), the MLA27 LRR domain might exert an inhibitory role in replacing ADP by ATP in the MLA-NBS. Thus, we propose that upon in planta effector recognition at the LRR domain and exchange of ADP by ATP in the NB-ARC domain, conformational changes in the self-interacting CC domains of MLA dimer enables downstream immune signaling (Figure 7).

We hypothesized that the MLA CC domain can serve as a template to predict CC dimer structures of other CNL-type R proteins provided they possess both significant sequence and secondary structure similarity. We selected *Arabidopsis* RPM1 for structure modeling, since its predicted CC domain fulfills these criteria (48.5% sequence similarity and matching structural profiles). RPM1 confers immunity to the bacterium *Pseudomonas syringae* expressing the AvrRpm1 effector (Grant et al., 1995), but it is unclear if RPM1 forms a homo-oligomer. Our modeling suggests that the RPM1 CC domain can form a dimer structure similar to MLA (Figure S5). Remarkably, the surface electrostatic properties seem to be preserved between the CC domains of MLA and RPM1, especially at the negatively charged helix α2a encompassing a conserved short region called the EDVID motif (Rairdan et al., 2008). This motif was shown to be involved in intradomain interactions between the CC and NBARC-LRR parts of the R protein Rx conferring immunity to potato virus X (Rairdan et al., 2008). The third and fourth positions within EDVID are mostly hydrophobic residues. Surprisingly, the EDVID motifs, which reside in the middle of helix α2a (Figure 1C), are positioned in the dimer exactly opposite of the "hinge" (between helix α2a and α2b) of the other protomer (Figure S5). The molecular dynamics (MD) simulation of the MLA CC dimer shows that the "hinge" flexibility leaves both EDVID motifs largely exposed on the same side of the dimer surface (Movie S1). The third and fourth residues in this motif point to the interior side of the MLA and RPM1 CC dimers, respectively. Indeed, Val80 of MLA, the fourth residue in the motif, contributes to hydrophobic interactions within the helix bundle of the dimer (Figure 2B), while the respective first, second, and fifth residues provide negative charges at the dimer surface in both MLA and RPM1 (Figure S5). Collectively these data suggest (1) that at least a subset of CNL-type R proteins can form CC homodimers and (2) that the EDVID motif together with the hinge region serve a role in connecting intra- and intermolecular receptor interactions to enable downstream immune signaling.

The induced proximity model was first proposed for an autoprocessing mechanism of caspase dimerization to initiate apoptosis by providing a close contact to monomeric procaspases (Salvesen and Dixit, 1999). Recently the CED-4 apoptosome has been proposed to act as a scaffold to induce proximity for caspase activation (Qi et al., 2010). Similar to the CED-4 apoptosome, Nod1 oligomerization enhances RICK self-association, and enforced homo-oligomerization of Nod1 is sufficient to activate the NF-κB transcription factor (Inohara et al., 2000).

In plants, N-terminal mediated Prf oligomer is proposed to induce proximity for the Prf coreceptors (Gutierrez et al., 2010). Recently, Krasileva et al. (2010) reported an effector-independent cell death induction triggered by the N-terminal TIR domain of RPP1 fused to wild-type GFP, but not by the TIR domain fused to a monomeric GFP, owing to a potentially enforced dimerization of the TIR domain by the dimerizing property of wild-type GFP. The crystal structure of the TIR domain of the flax L6 NLR revealed an interaction surface for TIR homodimerization, and the L6 TIR domain alone is both necessary and sufficient for immune signaling (Bernoux et al., 2011). Our results similarly demonstrate that the MLA CC dimer serves as minimal functional module in cell death initiation whose activity is tightly controlled in the context of the full-length receptor (Figures 6B and 6C). Since single amino acid substitutions impair both cell death activity and MLA CC dimerization (Figures 4C, 6B, and 6C), we presume that only properly folded MLA homodimers are able to trigger cell death in *N. benthamiana*. However, although unlikely, we cannot exclude the possibility that a portion of the heterologously expressed barley MLA receptor initiates cell death through association with the CC domain of *N. benthamiana* NLR proteins. We previously showed that the helix α1 of the MLA CC domain interacts with *Hv*WRKY1 and *Hv*WRKY2 transcription factors and that this interaction is enhanced in the presence of the cognate fungal effector (Shen et al., 2007). Since these WRKY transcription factors belong to a subgroup that can form hetero- or homo-oligomers with distinct roles in plant immune responses (Mangelsen et al., 2008; Xu et al., 2006), it is possible that effector-triggered conformational changes of MLA dimers induce proximity of particular WRKY oligomers for downstream signaling (Figure 7).

EXPERIMENTAL PROCEDURES

Expression and Purification of Recombinant Proteins

Native and selenomethionine (SeMet) derivative proteins of GST-MLA10 (5–120) were expressed in BL21 (DE3) strain (Novagen) at 15°C with 15 hr of isopropyl β-D-1-thiogalactopyranoside (IPTG) induction (0.3 mM). Native proteins and SeMet derivatives used for crystallization were expressed in LB and M9 medium, respectively. Cells were collected, pelleted and resuspended in buffer (25 mM Tris-HCl [pH 8.0], 150 mM NaCl, 3 mM DTT), lysed by sonication, and subsequently centrifuged at 25,000 *g* for 1 hr. The soluble proteins were first purified using glutathione-Sepharose4B resin (GE Healthcare) and the GST tag removed thereafter by PreScission protease. The processed proteins were further subjected to ion-exchange (Source-15Q, Pharmacia) and gel filtration (Superdex 200, Pharmacia) chromatography. Protein purification was performed at 4°C. The CC domain variants of MLA10 (5–120) were purified as described above. The purified CC variant proteins were subsequently separated on a gel filtration column (Superdex 75, Pharmacia) with a buffer containing 10 mM Tris-HCl (pH 8.0), 100 mM NaCl. Labeled 25.6 kDa chymotrypsin and 12.4 kDa cytchrome *c* were used as protein size marker. The recombinant wild-type CC domain (0.15 mM, 20 μL) was incubated with the homobifunctional crosslinker bis [Sulfosuccinimidyl] suberate (BS3) (20 mM, 5 μL) or ethylene glycolbis (sulfosuccinimidyl-succinate) (Sulfo-EGS) (20 mM, 10 μL) on ice for 2 hr in the reaction buffer containing 15 mM HEPES (pH 7.5) and 150 mM NaCl. The reaction was then quenched with 1.0 M Tris 7.5, 20 μl for 30 min, and the protein samples were separated via 15% SDS-PAGE.

The full-length MLA27-1 with an N-terminal His6 tag was amplified by standard PCR and cloned into pFAST-Bac1 (Invitrogen). The protein was expressed in SF21 cells for 48 hr at 28°C. The cells were lysed in the buffer (25 mM Tris-HCl [pH 8.0], 150 mM NaCl, and 10 μM ADP) by sonication. The extract was loaded onto Ni-NTA beads. MLA27-1 was further purified by anion ion exchange (Source-15Q, Pharmacia) with buffer (25 mM Tris-HCl [pH 8.0], 3 mM DTT) and buffer (25 mM Tris-HCl [pH 8.0], 1 M NaCl, 3 mM DTT). The protein was fractionated by gel filtration chromatography (Superdex 200, Pharmacia) with a buffer containing 10 mM Tris-HCl (pH 8.0), 100 mM NaCl, and 3 mM DTT.

Crystallization, Data Collection, Structure Determination, and Refinement

Native and SeMet derivative of MLA10 were concentrated in buffer containing 10 mM Tris-HCl (pH 8.0), 100 mM NaCl, and 3 mM DTT to 8 mg/ml for crystallization. Native protein was used for initial crystal screening and optimization. Native protein crystals were generated by mixing the protein with an equal amount of well solution (1.5 μl) by the hanging-drop vapor diffusion method. The native protein was crystallized in the buffer containing 0.1 M sodium acetate trihydrate (NaAc) (pH 4.6), 2.0 M sodium formate (NaCOOH) at 20°C. The anomalous diffraction data (Se-Peak) of SeMet was collected on beamline BL17U at Shanghai Synchrotron Radiation Facility (SSRF) and processed using the HKL-2000 package (Otwinowski and Minor, 1997).

The crystals belonged to space group $P2_12_12$. The ordered selenium sites were positioned by the program SOLVE (Terwilliger, 2000). The experimental electron density calculated with the initial SAD phases and modified with the program RESOLVE was sufficient for manual model-building under the program Coot (Emsley and Cowtan, 2004). The model was subsequently refined against the higher-resolution SeMet data set (to 2.0 Å) with the program Refmac (Murshudov et al., 1999).

Statistics of data collection, phasing, and structure refinement are given in Table S1.

Immunoprecipitation and Gel Filtration Chromatography, and Immunoblotting

Protein extraction, immunoprecipitation (IP), and gel filtration chromatography were essentially performed as described previously (Saijo et al., 2008) with the following modifications. Dynabeads M-280 Sheep anti-Rabbit IgG (Invitrogen), rabbit anti-Myc polyclonal antibody (Abcam, ab9106), and rabbit control IgG (Abcam, ab46540) were used for IP. Total leaf protein extract (5 mg) in 1 ml of the extraction buffer (Saijo et al., 2008) was rotated with 5 μg of the anti-Myc antibody or 5 μg of the rabbit control IgG for 1 hr at 4°C. Subsequently, antibody-protein complexes were captured by rotating with preblocked Dynabeads (~1×10^8 beads) for an additional 1 hr at 4°C according to the manufacturer's instructions. After washing, the antibody-protein complexes were eluted with 30 μl of 0.1 M glycine-HCl (pH 2.5) and neutralized with 3 μl of 1 M Tris-base. Immunoblotting was essentially performed as described previously (Bieri et al., 2004) except using Immobilon-P membrane (Millipore) and goat anti-Myc polyclonal antibody (Abcam, Ab9132) and anti-goat IgG conjugated with horseradish peroxidase (Abcam, Ab7125) for detection. Mouse anti-GFP monoclonal antibody (Clontech, 632381) and anti-mouse IgG conjugated with horseradish peroxidase (Abcam, ab20043) were used for detection of YFP fusion proteins.

Single-Cell Transient Expression Assay

Single-cell transient gene expression assays using biolistic delivery of plasmid DNA into plant epidermal cells were described previously (Shen et al., 2003). pUbi-GUS or p35S-mCherry was used for the reporter gene expression.

Statistical Analysis

Statistical analysis of haustorium index and electrolyte leakage was performed using R version 2.11.0. Unless otherwise indicated, data were evaluated by using analysis of variance (ANOVA) followed by Tukey-Kramer honestly significant difference test. A significant level of 0.01 was used for statistical analysis.

ACCESSION NUMBERS

Crystallographic coordinates of the MLA CC dimer have been deposited in the Protein Data Bank under the accession code PDB ID 3QFL.

SUPPLEMENTAL INFORMATION

Supplemental Information includes five figures, one table, one movie, Supplemental Experimental Procedures, and Supplemental References and can be found with this article at doi:10.1016/j.chom.2011.02.008.

ACKNOWLEDGMENTS

We thank Henk L. Dekker for help with the nucleotide-binding assay; Emiel Ver Loren van Themaat and Ulrike Göbel for help with R programming; Jane Parker for helpful comments on the manuscript; and Sabine Haigis, Petra Köchner, Elke Logemann, and Makoto Yoshikawa-Maekawa for technical assistance. This work was supported by funds from the Max Planck Society, a Deutsche Forschungsgemeinschaft grant (SFB670), the European Union BIOEXPLOIT grant (FOOD-CT-2005-513959), CNCSIS (ID-249 168/2007), POSDRU/89/1.5/S/60746, and the Knowledge Innovation Programme of the Chinese Academy of Sciences (KSCX2-YW-N-075), The National Outstanding Young Scholar Science Foundation of National Natural Science Foundation of China (20101331722).

Received: August 30, 2010
Revised: December 8, 2010
Accepted: February 7, 2011
Published: March 16, 2011

REFERENCES

Ade, J., DeYoung, B.J., Golstein, C., and Innes, R.W. (2007). Indirect activation of a plant nucleotide binding site-leucine-rich repeat protein by a bacterial protease. Proc. Natl. Acad. Sci. USA *104*, 2531–2536.

Azevedo, C., Sadanandom, A., Kitagawa, K., Freialdenhoven, A., Shirasu, K., and Schulze-Lefert, P. (2002). The RAR1 interactor SGT1, an essential component of *R* gene-triggered disease resistance. Science *295*, 2073–2076.

Bai, J., Pennill, L.A., Ning, J., Lee, S.W., Ramalingam, J., Webb, C.A., Zhao, B., Sun, Q., Nelson, J.C., Leach, J.E., and Hulbert, S.H. (2002). Diversity in nucleotide binding site-leucine-rich repeat genes in cereals. Genome Res. *12*, 1871–1884.

Bernoux, M., Ve, T., Williams, S., Warren, C., Hatters, D., Valkov, E., Zhang, X., Ellis, J.G., Kobe, B., and Dodds, P.N. (2011). Structural and functional analysis of a plant resistance protein TIR domain reveals interfaces for self-association, signaling and autoregulation. Cell Host Microbe *9*, this issue, 200–211.

Bieri, S., Mauch, S., Shen, Q.H., Peart, J., Devoto, A., Casais, C., Ceron, F., Schulze, S., Steinbiss, H.H., Shirasu, K., and Schulze-Lefert, P. (2004). RAR1 positively controls steady state levels of barley MLA resistance proteins and enables sufficient MLA6 accumulation for effective resistance. Plant Cell *16*, 3480–3495.

Chan, S.L., Mukasa, T., Santelli, E., Low, L.Y., and Pascual, J. (2010). The crystal structure of a TIR domain from *Arabidopsis thaliana* reveals a conserved helical region unique to plants. Protein Sci. *19*, 155–161.

Danot, O., Marquenet, E., Vidal-Ingigliardi, D., and Richet, E. (2009). Wheel of life, wheel of death: a mechanistic insight into signaling by STAND proteins. Structure *17*, 172–182.

Emsley, P., and Cowtan, K. (2004). Coot: model-building tools for molecular graphics. Acta Crystallogr. *60*, 2126–2132.

Grant, M.R., Godiard, L., Straube, E., Ashfield, T., Lewald, J., Sattler, A., Innes, R.W., and Dangl, J.L. (1995). Structure of the *Arabidopsis RPM1* gene enabling dual specificity disease resistance. Science *269*, 843–846.

Gutierrez, J.R., Balmuth, A.L., Ntoukakis, V., Mucyn, T.S., Gimenez-Ibanez, S., Jones, A.M., and Rathjen, J.P. (2010). Prf immune complexes of tomato are oligomeric and contain multiple Pto-like kinases that diversify effector recognition. Plant J. *61*, 507–518.

Inohara, N., Koseki, T., Lin, J., del Peso, L., Lucas, P.C., Chen, F.F., Ogura, Y., and Nunez, G. (2000). An induced proximity model for NF-kappa B activation in the Nod1/RICK and RIP signaling pathways. J. Biol. Chem. *275*, 27823–27831.

Jones, J.D., and Dangl, J.L. (2006). The plant immune system. Nature *444*, 323–329.

Kohn, W.D., Mant, C.T., and Hodges, R.S. (1997). α-helical protein assembly motifs. J. Biol. Chem. *272*, 2583–2586.

Krasileva, K.V., Dahlbeck, D., and Staskawicz, B.J. (2010). Activation of an Arabidopsis resistance protein is specified by the in planta association of its leucine-rich repeat domain with the cognate oomycete effector. Plant Cell *22*, 1–15.

Leipe, D.D., Koonin, E.V., and Aravind, L. (2004). STAND, a class of p-loop NTPases including animal and plant regulators of programmed cell death: multiple, complex domain architectures, unusual phyletic patterns, and evolution by horizontal gene transfer. J. Mol. Biol. *343*, 1–28.

Lukasik, E., and Takken, F.L. (2009). STANDing strong, resistance proteins instigators of plant defence. Curr. Opin. Plant Biol. *12*, 427–436.

Mangelsen, E., Kilian, J., Berendzen, K.W., Kolukisaoglu, U.H., Harter, K., Jansson, C., and Wanke, D. (2008). Phylogenetic and comparative gene expression analysis of barley (*Hordeum vulgare*) WRKY transcription factor family reveals putatively retained functions between monocots and dicots. BMC Genomics *9*, 194.

Mestre, P., and Baulcombe, D.C. (2006). Elicitor-mediated oligomerization of the tobacco N disease resistance protein. Plant Cell *18*, 491–501.

Murshudov, G.N., Vagin, A.A., Lebedev, A., Wilson, K.S., and Dodson, E.J. (1999). Efficient anisotropic refinement of macromolecular structures using FFT. Acta Crystallogr. *55*, 247–255.

Otwinowski, Z., and Minor, W. (1997). Processing of X-ray diffraction data collected in oscillation mode. Methods Enzymol. *276*, 307–326.

Qi, S., Pang, Y., Hu, Q., Liu, Q., Li, H., Zhou, Y., He, T., Liang, Q., Liu, Y., Yuan, X., et al. (2010). Crystal structure of the *Caenorhabditis elegans* apoptosome reveals an octameric assembly of CED-4. Cell *141*, 446–457.

Rairdan, G.J., Collier, S.M., Sacco, M.A., Baldwin, T.T., Boettrich, T., and Moffett, P. (2008). The coiled-coil and nucleotide binding domains of the Potato Rx disease resistance protein function in pathogen recognition and signaling. Plant Cell *20*, 739–751.

Saijo, Y., Zhu, D., Li, J., Rubio, V., Zhou, Z., Shen, Y., Hoecker, U., Wang, H., and Deng, X.W. (2008). Arabidopsis COP1/SPA1 complex and FHY1/FHY3 associate with distinct phosphorylated forms of phytochrome A in balancing light signaling. Mol. Cell *31*, 607–613.

Salvesen, G.S., and Dixit, V.M. (1999). Caspase activation: the induced-proximity model. Proc. Natl. Acad. Sci. USA *96*, 10964–10967.

Seeholzer, S., Tsuchimatsu, T., Jordan, T., Bieri, S., Pajonk, S., Yang, W., Jahoor, A., Shimizu, K.K., Keller, B., and Schulze-Lefert, P. (2010). Diversity at the *Mla* powdery mildew resistance locus from cultivated barley reveals sites of positive selection. Mol. Plant Microbe Interact. *23*, 497–509.

Shen, Q.H., and Schulze-Lefert, P. (2007). Rumble in the nuclear jungle: compartmentalization, trafficking, and nuclear action of plant immune receptors. EMBO J. *26*, 4293–4301.

Shen, Q.H., Zhou, F., Bieri, S., Haizel, T., Shirasu, K., and Schulze-Lefert, P. (2003). Recognition specificity and RAR1/SGT1 dependence in barley *Mla* disease resistance genes to the powdery mildew fungus. Plant Cell *15*, 732–744.

Shen, Q.H., Saijo, Y., Mauch, S., Biskup, C., Bieri, S., Keller, B., Seki, H., Ulker, B., Somssich, I.E., and Schulze-Lefert, P. (2007). Nuclear activity of MLA immune receptors links isolate-specific and basal disease-resistance responses. Science *315*, 1098–1103.

Shirasu, K. (2009). The HSP90-SGT1 chaperone complex for NLR immune sensors. Annu. Rev. Plant Biol. *60*, 139–164.

Shirasu, K., Lahaye, T., Tan, M.W., Zhou, F., Azevedo, C., and Schulze-Lefert, P. (1999). A novel class of eukaryotic zinc-binding proteins is required for disease resistance signaling in barley and development in *C. elegans*. Cell *99*, 355–366.

Takken, F.L.W., Albrecht, M., and Tameling, W.I.L. (2006). Resistance proteins: molecular switches of plant defence. Curr. Opin. Plant Biol. *9*, 383–390.

Tameling, W.I., Elzinga, S.D., Darmin, P.S., Vossen, J.H., Takken, F.L., Haring, M.A., and Cornelissen, B.J. (2002). The tomato *R* gene products I-2 and MI-1 are functional ATP binding proteins with ATPase activity. Plant Cell *14*, 2929–2939.

Tameling, W.I., Vossen, J.H., Albrecht, M., Lengauer, T., Berden, J.A., Haring, M.A., Cornelissen, B.J., and Takken, F.L. (2006). Mutations in the NB-ARC domain of I-2 that impair ATP hydrolysis cause autoactivation. Plant Physiol. *140*, 1233–1245.

Terwilliger, T.C. (2000). Maximum-likelihood density modification. Acta Crystallogr. *56*, 965–972.

van Ooijen, G., van den Burg, H.A., Cornelissen, B.J., and Takken, F.L. (2007). Structure and function of resistance proteins in solanaceous plants. Annu. Rev. Phytopathol. *45*, 43–72.

Xu, X., Chen, C., Fan, B., and Chen, Z. (2006). Physical and functional interactions between pathogen-induced Arabidopsis WRKY18, WRKY40, and WRKY60 transcription factors. Plant Cell *18*, 1310–1326.

Yu, X., Acehan, D., Menetret, J.F., Booth, C.R., Ludtke, S.J., Riedl, S.J., Shi, Y., Wang, X., and Akey, C.W. (2005). A structure of the human apoptosome at 12.8 A resolution provides insights into this cell death platform. Structure *13*, 1725–1735.